Real-time measurements of radon activity with the Timepix-based RADONLITE and RADONPIX detectors

2014 JINST 9 P11023

(http://iopscience.iop.org/1748-0221/9/11/P11023)

PUBLISHED BY IOP PUBLISHING FOR SISSA MEDIALAB

RECEIVED: *June 30, 2014*
ACCEPTED: *October 11, 2014*
PUBLISHED: *November 21, 2014*

Real-time measurements of radon activity with the Timepix-based RADONLITE and RADONPIX detectors

M. Caresana,[a] **L. Garlati,**[a] **F. Murtas,**[b,c] **S. Romano,**[a,c] **C.T. Severino**[c,d,1] **and M. Silari**[c]

[a] *Dipartimento di Energia, Politecnico di Milano, Via Ponzio 34/3, 20133 Milano, Italy*
[b] *INFN-LNF, Laboratori Nazionali di Frascati, Via Fermi 40, 00044 Frascati, Italy*
[c] *CERN, CH-1211 Geneva 23, Switzerland*
[d] *Universität Bern, LHEP, Sidlerstrasse 5, 3012 Bern, Switzerland*

E-mail: clizia.tecla.severino@cern.ch

ABSTRACT: Radon gas is the most important source of ionizing radiation among those of natural origin. Two new systems for radon measurement based on the Timepix silicon detector were developed. The positively charged radon daughters are electrostatically collected on the surface of the Si detector and their energy spectrum measured. Pattern recognition of the tracks on the sensor and particle identification are used to determine number and energy of the alpha particles and to subtract the background, allowing for efficient radon detection. The systems include an algorithm for real-time measurement of the radon concentration and the calculation of the effective dose to the lungs.

KEYWORDS: Hybrid detectors; Spectrometers; Dosimetry concepts and apparatus; Pattern recognition, cluster finding, calibration and fitting methods

[1] Corresponding author.

doi:10.1088/1748-0221/9/11/P11023

Contents

2014 JINST 9 P11023

1 Introduction

From a radiation protection point of view radon, a gas produced in the decay chain of ^{238}U, is the most important source of ionizing radiation among those of natural origin. Radon flows from rocks and soil and tends to concentrate in enclosed spaces like mines, cellars or houses. After smoking, radon is the second cause of lung cancer in the population [1]. When inhaled, the short-lived decay products ^{218}Po and ^{214}Po tend to deposit in the lungs where they emit highly ionizing alpha particles, which interact with biological tissue leading to DNA damage. The real-time measurement of radon levels is particularly useful in environmental monitoring campaigns, in which critical levels of radon concentration have to be verified promptly, or in the research of subterranean uranium mines. In order to achieve an accurate measurement of radon and of its concentration variation in a short time, a good real-time radon monitor should have a good sensitivity and should not be affected by the natural background.

Several systems based on semiconductor detectors and on the electrostatic collection of radon decay products have been developed [2–8]. This paper discusses the development of two new real-time radon detectors, called RADONLITE and RADONPIX, based on the very performing Timepix detector [9]. The Timepix is a pixelated hybrid semiconductor detector based on a universal read-out chip consisting of a 256×256 pixel ASIC that can be combined with different semiconductor sensors, allowing the identification and classification of the various particles and electromagnetic radiation in different categories. Each individual pixel in the sensor is connected to its own readout circuit, so that the signals can be collected and amplified and the data can be stored. The most used sensor is typically a layer of silicon 300 μm thick. Each pixel measures $55 \times 55\,\mu\text{m}^2$ for a total sensitive area of $1.4 \times 1.4\,\text{cm}^2$.

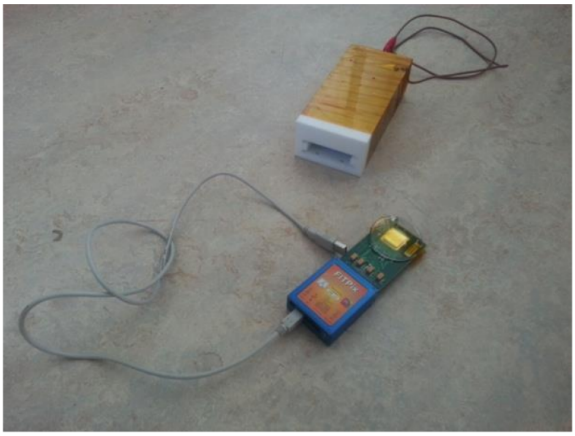

Figure 1. First prototype for the radon monitor. A standard Timepix [9] is placed inside a metallic box to which a high voltage is applied.

The RADONLITE and the RADONPIX offer advantages compared to other silicon detectors. They are light-weight portable devices allowing the real-time detection, on-line visualization and spectroscopic analysis of the different particles emitted by radon and its progeny. An ad-hoc pattern recognition algorithm allows for particle identification and background subtraction. The user can choose to measure either the alpha or the beta particles, or to carry out coincidence measurements. The ^{214}Po half-life of 164 μs is sufficiently short, in fact, that the ^{214}Bi/^{214}Po decays can be recognized as a coincidence. Both the RADONLITE and RADONPIX were tested and characterized in a reference radon chamber. The positively charged radon daughters are electrostatically collected on the silicon surface of the detectors and their energy spectrum is measured. After their characterization, the devices were tested in in-field measurements and compared with commercially available radon detectors.

2 Timepix for radon: first prototype

A performing radon monitor should have the spectroscopic capability of recognizing the alpha particles from the decay of ^{222}Rn, ^{218}Po and ^{214}Po. The idea underlying the present work is to employ the Timepix features combined with an appropriate cluster analysis and pattern recognition algorithm for the development of a system to measure the radon activity in real time. Timepix allows measuring the energy of the charged particle and performing the spectroscopic analysis of different types of particles. Being the ^{218}Po and ^{214}Po ions positively charged, the application of an external electric field forces them to attach to the sensor, improving the energy resolution and the sensitivity of the device. For this purpose, a first prototype consisting of a metallic electrostatic cell was built (see figure 1).

A standard Timepix was placed inside the cell where a number of holes let the radon enter. A set of measurements inside a reference radon chamber of 0.8 m^3 volume were carried out to investigate the influence of the electric field on the system efficiency and its reproducibility. The radon activity in the chamber was measured by an Alphaguard monitor [10]. A voltage variable between 0 and 1000 V was applied to the cell in order to intensify the collection of the radon progenies.

2014 JINST 9 P11023

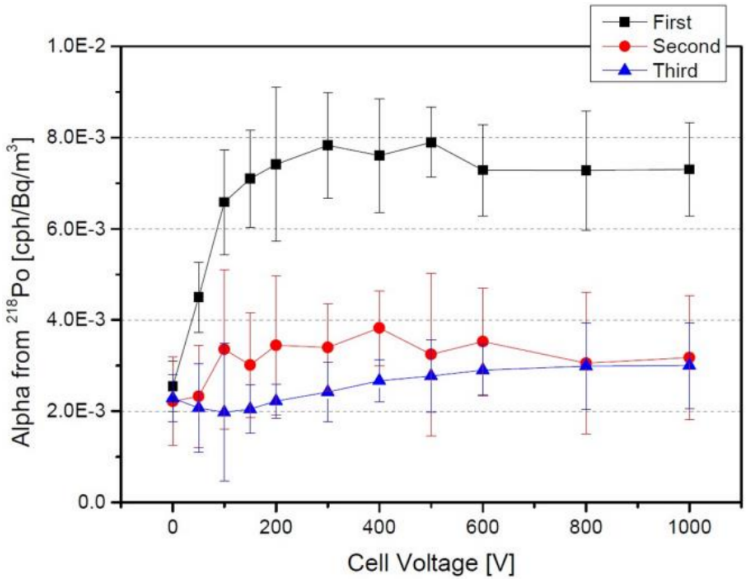

Figure 2. ^{218}Po alpha counts per hour normalized to the radon concentration as a function of the voltage applied to the cell for three different set of measurements. In this configuration the device does not guarantee the reproducibility of the measurement.

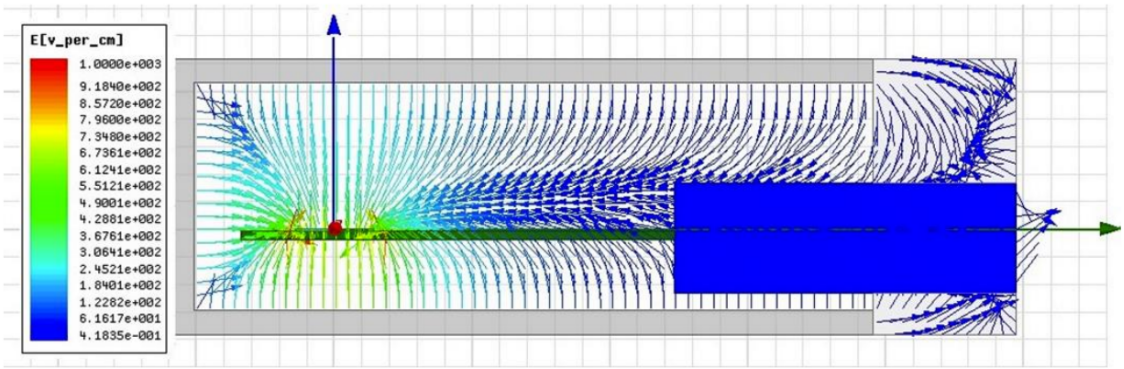

Figure 3. Electric field (in the ZY plane) simulation using the ANSYS Maxwell software [11].

A comparison of three different measurements is shown in figure 2. The results prove that this configuration is not stable enough and does not guarantee a good reproducibility. The reason for the system instability could be imputed to a non-homogeneity of the applied electric field. Figure 3 shows a simulation of this electric field made using the ANSYS Maxwell software [11]. In the proximity of the sensor the electric field is stronger, but it scatters the polonium ions on the board outside the silicon. Since the ions are not transported exclusively to the sensor, the system response from one measurement to another is subject to fluctuations that can lead to variations in the response. It was concluded that this first configuration was not suitable for a stable radon monitor and it needed to be modified. In order to develop an appropriate configuration allowing for a uniform application of the electric field, various alternatives were studied, which led to devising the RADONLITE and RADONPIX monitors described in the following.

2014 JINST 9 P11023

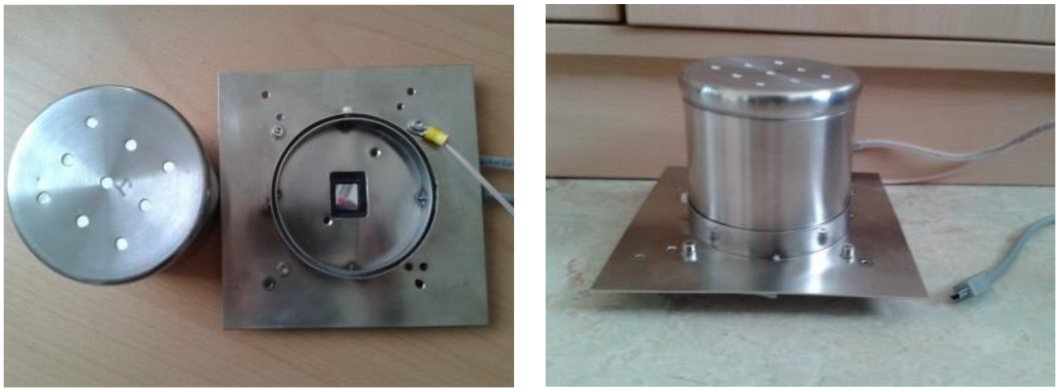

(a) (b)

Figure 4. The RADONLITE: the LITE version of Timepix [13] is placed in the center of a metallic base on top of which a metallic cylinder rests.

3 RADONLITE and RADONPIX

The RADONLITE is a modified version of the cell used by A. Frojdh and et al. [3] (figure 4). The device consists of a conductive cylinder resting on a conductive base, with the silicon detector mounted in the centre. Holes were drilled on the top of the cylinder to let radon diffuse inside the cell. To ensure the radon equilibrium and to prevent the radon daughters to enter the system, the holes were closed with a Millipore filter paper [12]. The detector is the LITE USB version of Timepix [13], in which the chip is mounted on a single printed circuit board of $15 \times 60\,\mathrm{mm}^2$ and is coupled with a p-n silicon sensor $300\,\mu\mathrm{m}$ thick. Radon diffuses into the cylinder where it decays to ^{218}Po emitting an alpha particle. The electric field for the electrostatic collection of the radon daughters is created by applying a potential difference between the conductive walls and the LITE sensor. An ANSYS Maxwell simulation of the electric field was performed in order to investigate the electric field propagation inside the metallic cell of the RADONLITE and to better understand how this field influences the alpha distribution on the silicon sensor (figure 5). Although the electric field is more intense in the proximity of the sensor centre, this configuration seems to be more promising than the previous one because of the losses reduction. In order to ensure a better distribution of the electric field a further monitor, called RADONPIX, was developed. The device, shown in figure 6, consists of a G10 fiberglass frame of $10 \times 10\,\mathrm{cm}^2$ on top of which a board equipped with a metallic mesh screen with $50\,\mu\mathrm{m}$ holes is placed [14]. The frame encloses a QUAD Timepix, in which four single chips are placed on a $2 \times 2\,\mathrm{cm}^2$ matrix covering a $2.8 \times 2.8\,\mathrm{cm}^2$ active area using one common silicon sensor $300\,\mu\mathrm{m}$ thick with 512×512 pixels. The electric field for the electrostatic collection of radon progeny is applied to the RADONPIX by means of the mesh screen, which is placed 2 cm upon the QUAD sensor. The radon enters the system volume through the holes of the screen, which also ensures the radon equilibrium inside the detector preventing the entrance of ^{218}Po and ^{214}Po ions. Both the USB LITE and the QUAD are driven by the Pixelman software [15].

2014 JINST 9 P11023

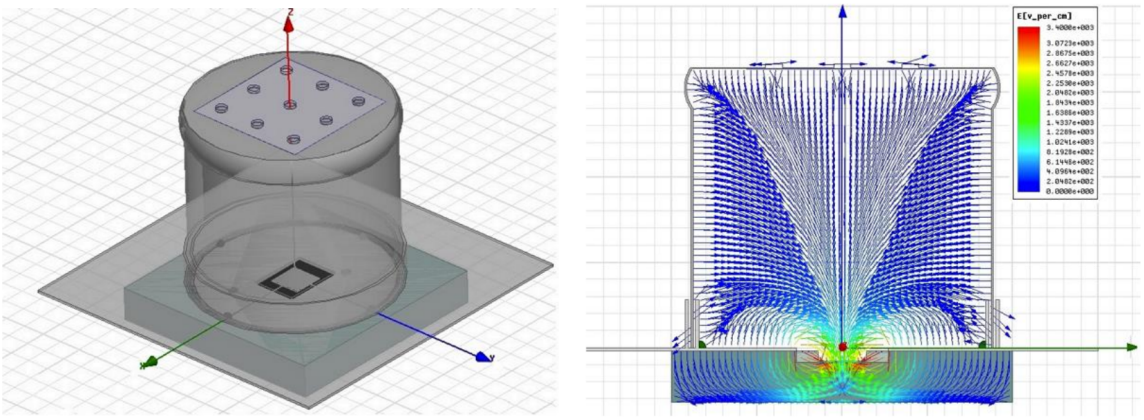

(a) (b)

Figure 5. Electric field simulation for the RADONLITE with the ANSYS Maxwell software [11]. (a): sketch of the system; (b): electric field in the ZY plane.

(a) (b)

Figure 6. The RADONPIX: the Timepix QUAD (a) is closed with a metallic mesh screen [14] that is used to apply the electric field and to ensure the radon equilibrium.

4 Measurements and results

The influence of the electric field on the RADONLITE and RADONPIX sensitivity was investigated by a series of measurements inside the reference radon chamber.

In order to improve the collection of the radon progenies, a voltage variable between 0 and 6000 V was applied to the RADONLITE and a voltage between 0 and 2000 V was applied to the RADONPIX. The bias voltage of the Timepix sensors was kept at 100 V in all measurements, ensuring the complete depletion of the silicon sensor. The measurements were carried out in TOT (Time Over Threshold) mode, which allows information about the particles energy to be obtained.

4.1 Pattern recognition and discrimination

Different types of ionizing particles create different types of hit clusters in the Timepix sensor because of the different dE/dx. Thereby, by analysing the properties of the clusters these can be

2014 JINST 9 P11023

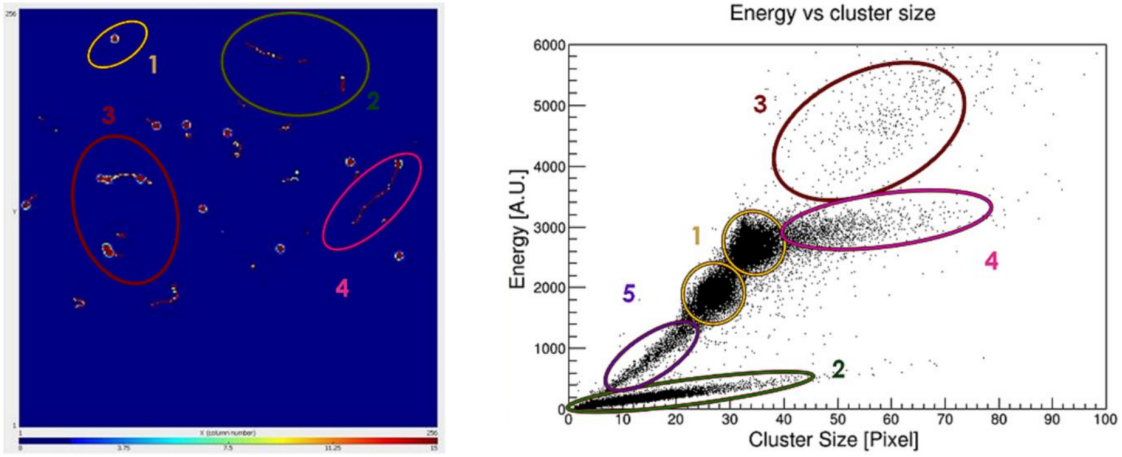

Figure 7. RADONLITE. Left: 2 s frame from Pixelman acquisition software [15], showing the different particle populations. Right: energy (in arbitrary units) versus the cluster size.

classified and assigned to a specific particle category. According to these considerations, a particle identification algorithm was developed, which allows performing an event-by-event analysis and background suppression. The algorithm uses the MAFalda (Medipix Analysis Framework) code, based on C^{++} language and ROOT package [16, 17]. In order to discriminate the track and attribute it to the particle the angular information, the deposition of energy and the cluster morphology have been studied and several characteristics were computed for each cluster, such as total deposited energy, length and width of a bounding box and the cluster density. The first step in the data analysis is to search for any dead/noisy pixels. This is done by binning all the data acquired into a single array, and looking for pixels that have a much higher aggregate number of hits than the average. These pixels are then masked for the remaining analysis. A more sensitive approach is to bin the number of single pixel hits for each pixel and look for pixels that have substantially higher counts than the average. The data is then sorted into so called clusters. The algorithm starts by looking for cells that have received hits. When it finds one it creates a new cluster. It then recursively searches the 8 cells surrounding that cluster and if they have received hits they are added to the cluster. In principle a cluster should be track left by a single particle, however clusters can contain multiple tracks if they overlap. Figure 7 shows a 2 s frame acquired with the RADONLITE.

The circles 1 in the figure highlight the tracks (blobs) due to the ^{218}Po and ^{214}Po alpha decays, circles 2 indicate the beta decay (curly tracks) of ^{214}Pb and ^{214}Bi, circles 3 show overlapping tracks, while the alpha and beta coincidence emission is indicated by circles 4. The decay of ^{214}Po, in fact, occurs 164 μs after the decay of ^{214}Bi and this produces a blob due to the alpha particles with a tail due to the beta. The same figure shows a scatter plot of the energy versus the cluster size, in which the different particle populations are clearly distinguishable. Through an appropriate clustering a cut on the alpha particle population can be applied in order to eliminate the beta contribution. Figure 8 shows the scatter plot of alpha particles after the cut for the RADONLITE. A selection of clusters according to cluster size and energy allows suppressing the signal coming from any other source, and thus an effective suppression of the background. This kind of pattern recognition leads

2014 JINST 9 P11023

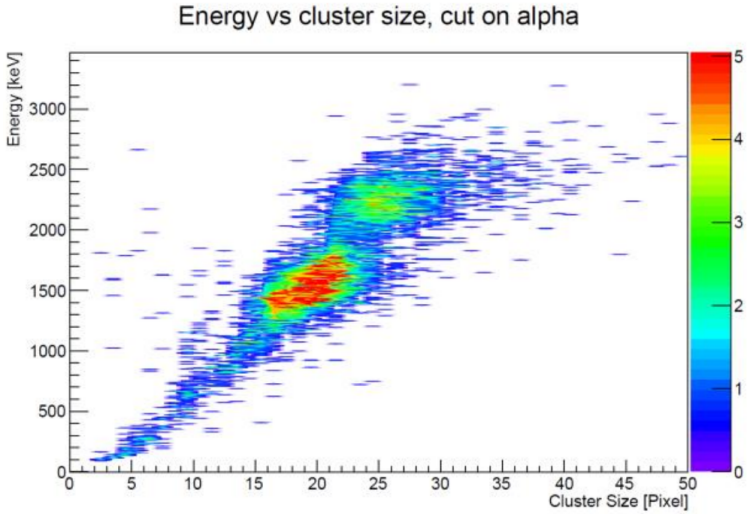

Figure 8. RADONLITE. A cut on alpha particle population is possible thought an appropriate selection of clusters according to cluster size and energy.

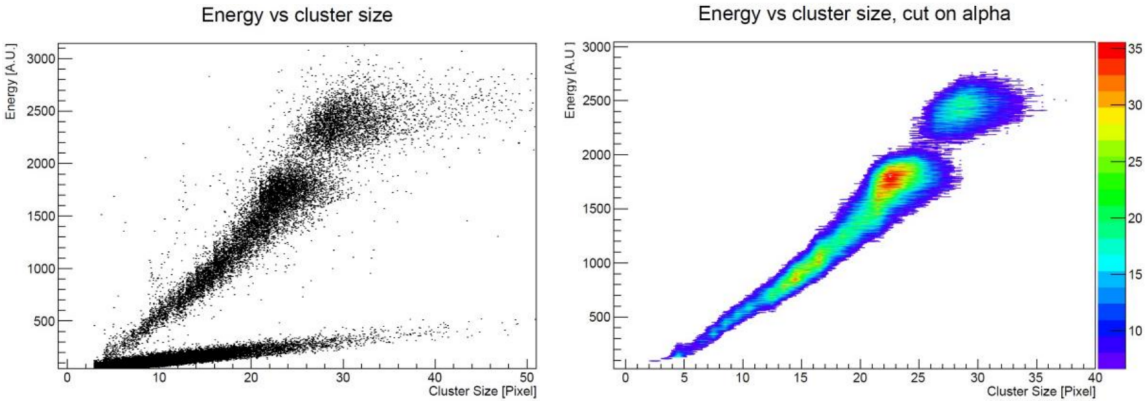

(a) (b)

Figure 9. RADONPIX. Scatter plot of TOT counts as a function of the cluster size for all particles (a) and with the cut on the alpha population (b).

to obtain a stable system that can be employed for fast as well as for long radon measurements. The scatter plot of the TOT counts versus the cluster size obtained from a measurement with the RADONPIX is shown in the figure 9(a). The separation between alpha and beta families is clear also in this case. By applying the cut on the alpha family two alpha particle populations are selected, as shown in the plot of figure 9(b).

4.2 Spectrum of radon progeny

Figure 10(a) shows the spectrum of the two alpha particles from radon decay measured by the RADONLITE. The ^{218}Po at 6 MeV and the ^{214}Po at 7.69 MeV can be easily identified. The alpha energy spectrum measured by the RADONPIX is shown if figure 10(b), but in this case the spectrum has a tail which can be attributed to the 5.5 MeV alpha particles from ^{222}Rn. In

2014 JINST 9 P11023

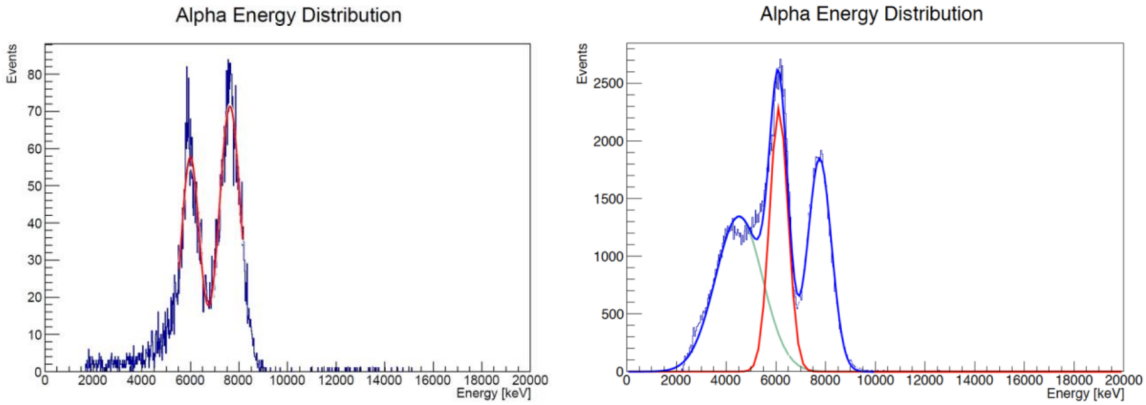

(a) (b)

Figure 10. (a) The radon progeny energy spectrum measured by the RADONLITE showing the alpha particles from ^{218}Po at 6 MeV and from ^{214}Po at 7.69 MeV peaks. (b) Energy distribution of alpha particles from radon decay measured by the RADONPIX. The peaks at 6 MeV and 7.69 MeV are easily recognizable with a third peak at lower energy probably due to the detection of alpha from the direct decay of radon or to a possible contamination from ^{210}Po.

the RADONPIX, in fact, the air gap between the screen and the silicon sensor is 2 cm and so the probability to detect also the alpha particles coming from the direct decay of radon is quite high. In the RADONLITE the probability to see the direct decay of alpha particles from radon is lower due to the 8 cm air gap between the top of the cylinder and the silicon sensor. Due to the air volume seen by the RADONPIX sensor, the alpha particles from ^{222}Rn are expected to have an energy distribution centered at about 4 MeV. The peak could also be due to a possible contamination from ^{210}Po. The latter needs to be investigated and further studies are currently in progress. However, the contribution due to the peak at 4 MeV can be eliminated by fitting the energy distribution with a Gaussian that is the sum of three Gaussians. The integral of the Gaussian fitting the peak at 6 MeV (in red in figure 10(b)) gives the number of alpha particles from the ^{218}Po decay.

4.3 Working points and calibration factors

The alpha particle counts per hour normalized to the radon concentration as a function of the electric field applied to the systems are shown in figure 11(a) for the RADONLITE and in figure 11(b) for the RADONPIX. The total alpha particle counts are shown in blue, the alpha particles coming from the decay of ^{214}Po in red and the counts due to ^{218}Po in black. The error bars were computed by means of the error propagation formula. After the radon emanates it takes a couple of hours before the short-lived radon decay products come into full equilibrium inside the detector. Nevertheless, the first decay product, ^{218}Po, achieves full equilibrium with radon very quickly (in about 15 minutes). In order to use the RADONLITE and the RADONPIX for a fast monitoring of the radon presence, just the alpha particles from ^{218}Po are taken into account. Figures 11 also shows the counts from ^{218}Po decay as a function of the voltage applied to the RADONLITE (figure 11(c)) and to the RADONPIX (figure 11(d)) for different sets of measurements. The two devices ensure a good reproducibility of the measurements. The working point of the RADONLITE was set at 3400 V, that of RADONPIX at 1400 V. The device calibration factors are given by the number

2014 JINST 9 P11023

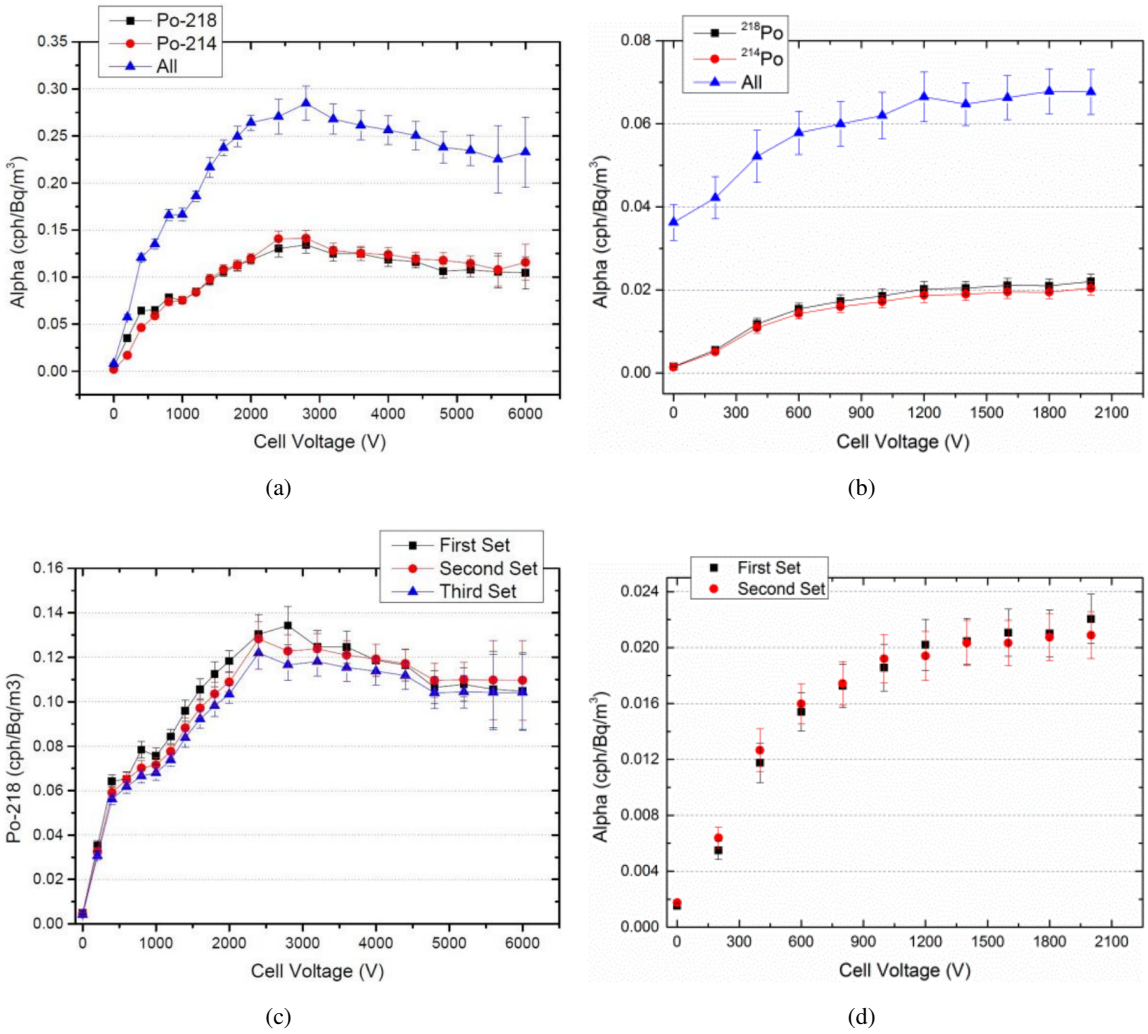

Figure 11. Counts per hour normalized to the radon concentration versus the voltage applied to the RADONLITE (a) and to the RADONPIX (b). In blue the counts coming from all detected alpha particles, in red the counts due to the ^{214}Po alpha particles and in black those due to the ^{218}Po decay. The counts from ^{218}Po decay per hour normalized to the radon concentration as a function of the voltage applied to the RADONLITE (c) and to the RADONPIX (d) for different sets of measurements.

of alpha particles counted by the systems over the reference radon concentration measured by the Alphaguard monitor. The calibration factor at the working point is $0.124 \pm 8\%$ cph/Bq/m^3 for the RADONLITE and $0.02 \pm 8\%$ cph/Bq/m^3 for the RADONPIX. An evidence of the RADONLITE and RADONPIX stability can be seen in figure 12, which shows the position of the 6 MeV and 7.69 MeV peaks and their standard deviation as a function of the voltage applied to the systems. In both cases, the figure shows that varying the applied voltage does not shift the peak position and increasing the electric field yields a slightly better resolution of the peaks.

In figure 13 the radon concentration measured by the RADONLITE (figure 13(a)) and RADONPIX (figure 13(b)) is compared with the reference value measured by the Alphaguard inside the radon chamber. In figure 13(a) each point gives the average concentration measured in 10 min-

2014 JINST 9 P11023

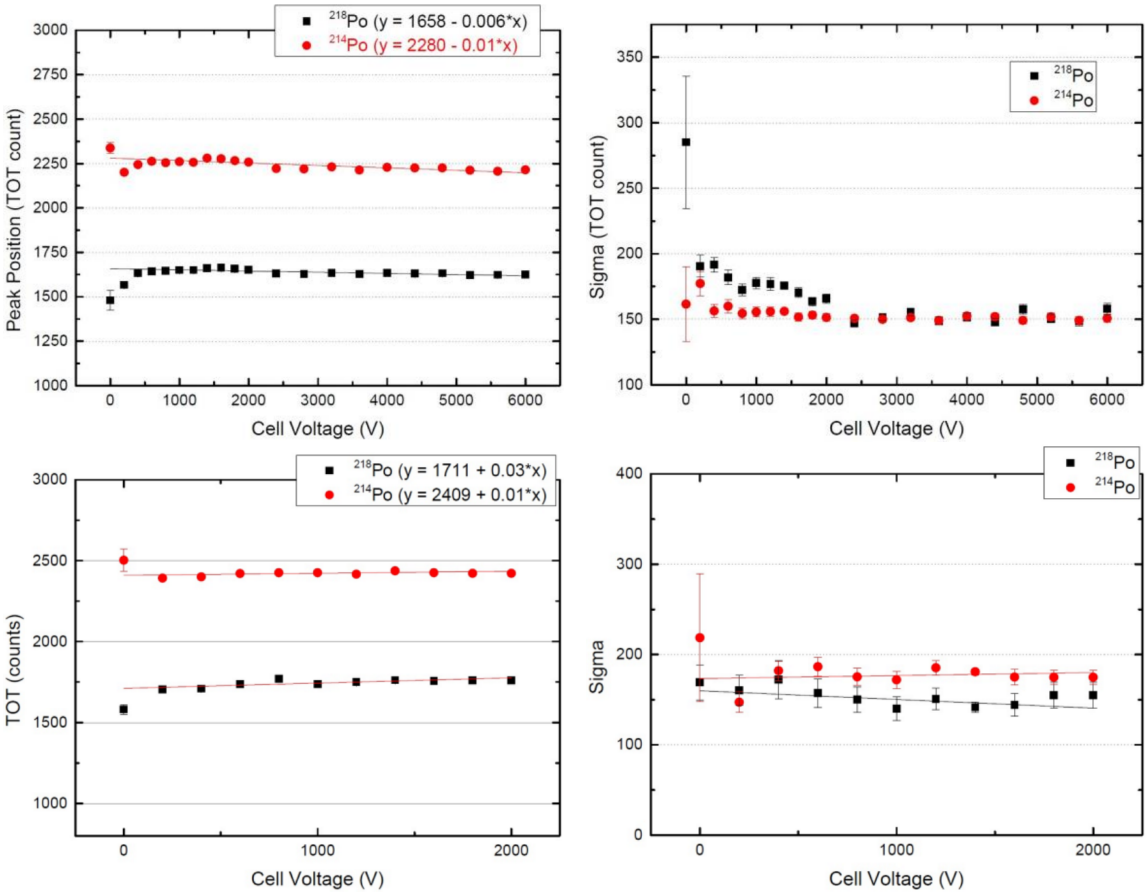

Figure 12. The peaks position of ^{218}Po and ^{214}Po and their standard variation as a function of the electric field applied to the RADONLITE (on the top) and to the RADONPIX (on the bottom).

utes while in figure 13(b) each point of the plot gives the one-hour average of the radon concentration. As evident from the figures, both the RADONLITE and the RADONPIX show a good agreement with the Alphaguard.

The new radon detectors are able to follow the radon variation correctly, although the RADONPIX shows larger fluctuations in the concentration measurement due to its small active volume and its small sensitivity. Table 1 [18–21] compares the technical specifications of RADONLITE and RADONPIX to those some of the most used commercial active radon detectors. The new radon devices show a ^{218}Po sensitivity (in cph/Bq) comparable to the other detectors but offer a higher portability.

4.4 Software plug-in for on-line monitoring

To make the RADONLITE and the RADONPIX more performing, a Python [22] scripting plug-in for online monitoring was developed, which allows the Pixelman functionality to be enhanced thanks to the use of the Python libraries. The plug-in, in fact, embeds a Python interpreter into Pixelman so that its functionality can be controlled from a Python script, which has access to all Pixelman application programming interface (API) [23]. The Radon Monitoring plug-in developed

2014 JINST 9 P11023

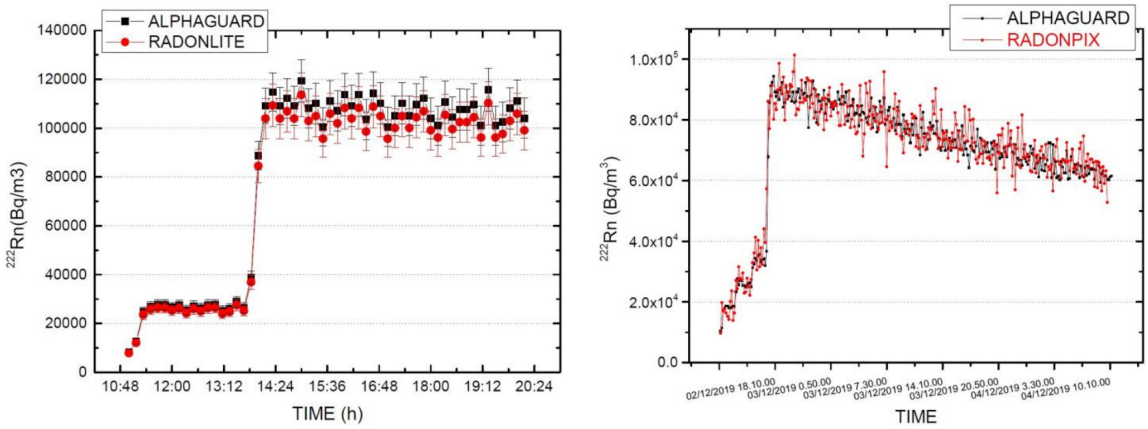

Figure 13. Two different measurements with RADONLITE (a) and RADONPIX (b) inside the radon chamber during which the radon concentration was varied. The radon concentration in Bq/m^3 present inside the radon chamber measured by the new radon monitors and by the Alphaguard are compared. The HV of the RADONLITE is at 3400 V, the one of RADONPIX is at 1400 V.

Table 1. Technical specification of RADONLITE, RADONPIX and some of the most used commercial active radon detectors [18–21].

Radon monitor	*Detector type*	*Total/active volume*	*Weight* (kg)	*Sensitivity* (cph/Bq/m^3)	^{218}*Po sensitivity per unit active volume* (cph/Bq)
RADONLITE	Semiconductor detector	650 cm^3/510 cm^3	0.6	0.124	243
RADONPIX	Semiconductor detector	180 cm^3/120 cm^3	0.53	0.02	165
ALPHAGUARD	Pulse ionisation chamber	620 cm^3/560 cm^3	4.5	3	2679
RAD7	Semiconductor detector	17695 cm^3/700 cm^3	5	0.4	286
RADIM 5B	Semiconductor detector	2700 cm^3/1400 cm^3	0.5	0.3	107
RADHOME_HRE	Semiconductor detector	76800 cm^3/n.s.	20	0.6	–
PYLON AB6	Lucas cell	14260 cm^3/424 cm^3	6	1.26	1486

in the present work allows to automatically set-up the detector and to perform data acquisition, hit clustering and particle ID. In particular, the real-time monitoring of the radon concentration, the effective dose-to-lung rate and the energy distribution of the particles produced during the radon decay are displayed in a pop-up window of the acquisition laptop. A screen-shot of the pop-up window from the Radon Monitoring plug-in during an acquisition with the RADONLITE is shown in figure 14. In the top plot the real-time radon concentration is displayed. The middle plot shows the average radon concentration calculated every 10 minutes. This information is also reported in numerical format. The bottom plot shows the energy distribution of the alpha particles to check that the detected radiation is actually radon. The plug-in also gives information about the effective dose rate (in μSv/h) and the cumulative dose (in μSv) in numerical format. The on-line data analysis is

2014 JINST 9 P11023

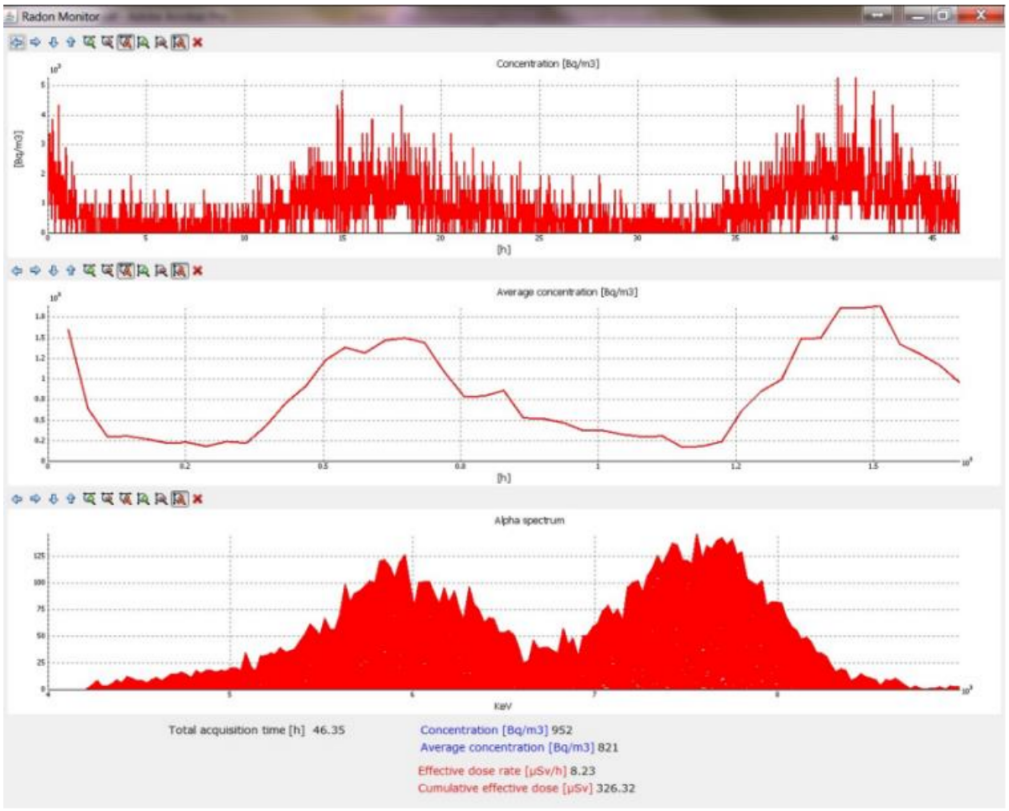

Figure 14. Screen-shots of the Radon Monitor plug-in during a measurement with the RADONLITE in the basement of the Polytechnic of Milan. See text for details.

possible via the Pixelman cluster analysis libraries. The results are further analyzed according to the principles of pattern recognition of the MAFalda algorithm. Moreover, before each acquisition the Radon Monitor plug-in enables the automatic check of the device, making sure that the right configuration is being used. Firstly, the software checks the cluster rate taking into account that this should be below 50 clusters/frame (so that cluster overlapping is avoided), and suggests the user the optimal acquisition time per frame accordingly. Cluster overlap in fact leads to errors in the particle recognition. The effective dose is calculated assuming that the activities of ^{222}Rn, ^{218}Po, ^{214}Pb and ^{214}Bi are in the ratio of $1 : 0.9 : 0.45 : 0.225$ [24, 25], corresponding to an equilibrium factor F of 0.4, which is a reasonably typical domestic value. A conversion factor of 9.0×10^{-6} mSv/h per Bq/m^3, a radiation weighting factor of 20 for the alpha particles and a tissue weighting factor of 0.12 for the lung were taken into account.

5 In-field measurements

After the system characterization in the radon chamber, in-field measurements in a number of representative locations were carried out with both the RADONLITE and the RADONPIX. The measurements were performed in the basement of the Polytechnic of Milan (POLIMI), Italy; in two house cellars in Thoiry (FRANCE1) and in Saint Genis Pouilly (FRANCE2), located in the French region close to CERN; and in three different locations at CERN: the ion source room of the old

2014 JINST 9 P11023

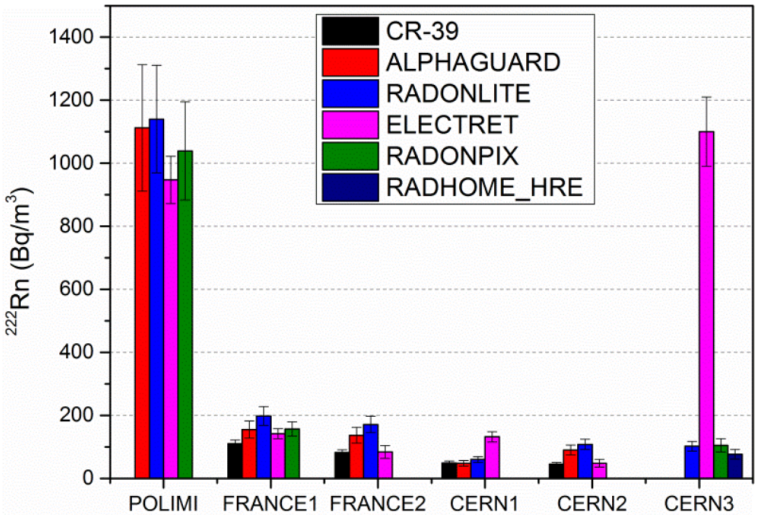

Figure 15. Results from in-field comparison measurement between RADONLITE, RADONPIX, Alphaguard, electret and CR-39. The CR-39 measurement is not directly comparable with the measurements of the other devices, since the CR-39 was exposed to radon in a different lapse of time.

CERN 600 MeV synchro-cyclotron (CERN1) [26], the basement of an office building (CERN2) and in a laboratory equipped with radioactive sources where all CERN radiation detectors are periodically calibrated (CERN3). An Alphaguard monitor and an electret were used in order to compare the RADONLITE and the RADONPIX with commercial radon detectors. In CERN calibration laboratory the measurements were carried out with the RADONLITE, the RADONPIX, the electret and the RADHOME_HRE [18].

Before employing the RADONLITE and the RADONPIX in in-field tests, a measurement of about six months was carried out with CR-39 passive dosimeters in some of the places listed above, in order to acquire preliminary information of the radon level. The CR-39 measurements are not directly comparable with the measurements of the other devices, since the CR-39 dosimeters were exposed in a different lapse of time. Figure 15 summarizes the results of all in-field measurements, revealing a good agreement between the RADONLITE, the RADONPIX and the commercial radon detectors. Unfortunately, during the measurement performed in CERN calibration laboratory some gamma and neutron sources were in use and the corresponding gamma background invalidated the electret response, which gives a too high value. Nevertheless, the gamma background did not affect the RADONLITE and RADONPIX measurements, proving the good background suppression performed by the cluster analysis. The good agreement between the new radon systems and the Alphaguard can be seen in figure 16, which compares the radon concentration measured by the three devices during the measurement performed at POLIMI. As evident from the figure, the RADONLITE and the RADONPIX are still able to follow the radon variation very well. However, the RADONPIX seems to be more susceptible to statistical fluctuations, as already shown in figure 13. The measurement is also a good example of how the operation of the ventilation system can influence the accumulation of radon. The peaks of maximum concentration, in fact, occur during the night or during the weekend (see the final part of the plot), when the ventilation system is turned off.

2014 JINST 9 P11023

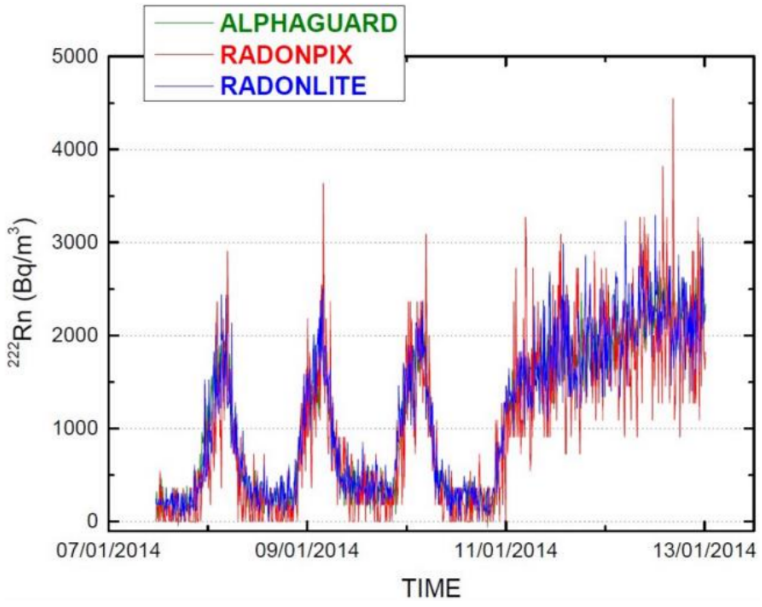

Figure 16. Radon concentration in Bq/m^3 measured by the RADONLITE, the RADONPIX and the Alphaguard.

6 Conclusions

The present results show that the RADONLITE and the RADONPIX are good candidates for real-time radon monitoring, thanks to the features of the Timepix sensor combined with a proper design of the instrument and an appropriate cluster analysis and pattern recognition algorithm. Both devices were characterized in a reference radon chamber: a calibration factor of 0.125 cph/Bq/m^3 for the RADONLITE and of 0.02 cph/Bq/m^3 for the RADONPIX were determined.

The systems were also tested in in-field measurements and the results are in good agreement with those of the commercial units Alphaguard, electret and RADHOME_HRE. The development of the Radon Monitoring plug-in makes the RADONLITE and the RADONPIX more performing due to the automatic control of the acquisition data and on-line data analysis. The real-time monitoring of the radon concentration, the effective dose-to-lung rate and the energy distribution of the particles produced during the radon decay are shown in a pop-up window of the acquisition laptop. Future improvements of the two instruments entail the insulation of the systems and the employment of a dedicated circuit for the application of the high voltage. Since radon daughters detection can be influenced by environmental factors, such as pressure, humidity and temperature, the introduction of sensors to monitor these parameters combined with an extension of the Radon Monitoring plug-in for the on-line visualization are planned. The sensitivity of the two systems can be increased by adopting specific solutions. For example, an improvement of the RADONLITE electric field employing a field cage and making an improvement of the base in which the LITE is resting should lead to a better distribution of the polonium ions on the sensor, yielding a higher sensitivity. In the RADONPIX, a higher volume and a pump flowing the air inside the system should also improve the instrument performance.

2014 JINST 9 P11023

References

[1] H. Zeeb and F. Shannoun, *WHO handbook on indoor radon — a public health perspective*, World Health Organization (2009), ISBN 9789241547673, http://www.who.int/ionizing_radiation/env/radon/en/index1.html.

[2] N. Noto, H. Ohsumi and S. Kobayashi, *Performance of the electrostatic collection type radon and toron detector*, *IEEE Nucl. Sci. Symp. Conf. Rec.* **1** (2002) 429.

[3] A. Fröjdh, G. Thungström, C. Fröjdh and S. Petersson, *An optimized system for measurement of radon levels in buildings by spectroscopic measurement of radon progeny*, 2011 *JINST* **6** C12018.

[4] S. de Martino, C. Sabbarese and G. Monetti, *Radon emanation and exhalation rates from soils measured with an electrostatic collector*, *Appl. Radiat. Isotopes* **49** (1998) 407.

[5] P.K. Hopke, *Use of electrostatic collection of* ^{218}*Po for measuring Rn*, *Health Phys.* **57** (1989) 39.

[6] M.E. Bacon, *A comparison of electrostatic and filtered air collection of radon progeny*, *Eur. J. Phys.* **25** (2004) 239.

[7] V. Roca et al., *A monitor for continuous and remote control of radon level and environmental parameters*, *IEEE Nucl. Sci. Symp. Conf. Rec.* **3** (2004) 1563.

[8] M. Wójcik and L. Morawska, *Radon concentration and exhalation measurement with a semiconductor detector and an electrostatic precipitator working in a closed circulation system*, *Nucl. Instrum. Meth.* **212** (1983) 393.

[9] X. Llopart, R. Ballabriga, M. Campbell, L. Tlustos and W. Wong, *Timepix, a 65k programmable pixel readout chip for arrival time, energy and/or photon counting measurements*, *Nucl. Instrum. Meth.* **A 581** (2007) 485.

[10] http://saphymo.de//products/alpha_slides.html.

[11] http://www.ansys.com/Products/Simulation+Technology/Systems+&+Multiphysics/Multiphysics+Enabled+Products/ANSYS+Maxwell.

[12] http://www.millipore.com.

[13] Z. Vykydal and J. Jakubek, *USB Lite — miniaturized readout interface for Medipix2 detector*, *Nucl. Instrum. Meth.* **A 633** (2011) S48.

[14] F. Sauli, *GEM: a new concept for electron amplification in gas detectors*, *Nucl. Instrum. Meth.* **A 386** (1997) 531.

[15] D. Tureček, T. Holy, J. Jakubek, S. Pospisil and Z. Vykydal, *Pixelman: a multi-platform data acquisition and processing software package for Medipix2, Timepix and Medipix3 detectors*, 2011 *JINST* **6** C01046.

[16] https://twiki.cern.ch/twiki/bin/view/Main/MAFalda.

[17] http://root.cern.ch/drupal/.

[18] http://www.algade.com/index.php/Mesure-en-continu-du-radon/mesure-continue-radon-hre.html.

[19] http://www.durridge.com/products_rad7.shtml.

[20] http://plch-smm.com/radim5b.php.

[21] http://www.pylonelectronics.com/pylonAB6monitor.php.

[22] https://www.python.org/.

2014 JINST 9 P11023

[23] D. Tureček, *Manual of Python scripting for Pixelman*, http://aladdin.utef.cvut.cz/ofat/others/Plugins/Python_scripting.html.

[24] UNESCEAR, *Sources and effects of ionizing radiation*, United Nations University Press (2000).

[25] ICRP, *Protection against radon-222 at home and at work*, ICRP Publication 65, *Ann. ICRP* **23** (1993), http://www.icrp.org/publication.asp?id=ICRP Publication 65.

[26] B.W. Allardyce, A. Fiebig, G. Le Dallic, J.H.B. Madsen and P.H. Standley, *Status report on CERN SC*, *IEEE Trans. Nucl. Sci.* **26** (1979) 1979.

2014 JINST 9 P11023